Overview of the FTU Results

A. A. Tuccillo 1) on behalf of FTU Team[*] and
L. Amicucci 2),   A. Biancalani 3,4),   A. Bierwage 5),   G. Breyannis 2)   I. Chavdarovski 6),
L. Chen 7,8),   F. De Luca 9),   Z. O. Guimarães-Filho 10),   A. Jacchia 11),   E. Lazzaro 11),
F. Pegoraro 12), M. Romanelli 13), G. Szepesi 14), X. Wang 7,8)

1) Associazione Euratom-ENEA sulla Fusione, C.R. ENEA-Frascati, Via E. Fermi 45, 00044
   Frascati, Roma, Italy
2) ENEA Fellow, C.R. ENEA-Frascati, Via E. Fermi 45, 00044
   Frascati, Roma, Italy
3) Max-Planck-Institut für Plasmaphysik, Euratom Association, Boltzmannstraße 2, D-85748
   Garching, Germany
4) Max-Planck-Institut für Sonnensystemforschung, Katlenburg-Lindau, Germany
5) Japan Atomic Energy Agency, 801-1, Mukouyama, Naka, Ibaraki-ken 311-0193, Japan
6) National Fusion Research Institute, Gwahangno 113, Yuseong-gu, Daejeon 305-333, Korea
7) Department of Physics and Astronomy, University of California, Irvine, CA 92697-2575
8) Institute for Fusion Theory and Simulation, Zhejiang University, Hangzhou 310027, P.R.C.
9) Università di Milano, Dipartimento di Fisica, via Celoria 16, 20133- Milano, Italy
10) PIIM, Université de Provence, Marseille, France
11) Associazione Euratom-ENEA sulla Fusione, IFP-CNR, Via R. Cozzi 53, 20125 Milano,
    Italy
12) Department of Physics, University of Pisa, 56127 Pisa, Italy
13) Euratom-CCFE Association, Culham Science Center, OX143DB, UK
14) CFSA University of Warwick, CV47AL, UK

e-mail contact of main author: angelo.tuccillo@enea.it

Abstract. New FTU ohmic discharges with Liquid Lithium Limiter at $I_P = 0.7$-0.75 MA, $B_T = 7$ T, $n_{e0} \geq 5 \, 10^{20}$m^{-3}, confirm the spontaneous transition to an enhanced confinement regime, 1.3-1.4 times ITER-97-L, when the density peaking factor is above a threshold value of 1.7-1.8. The improved confinement derives from a reduction of electron thermal conductivity (χ_e) as density increases, while ion thermal conductivity (χ_i) remains close to neoclassical values. Linear microstability reveals the importance of lithium in triggering a turbulent inward flux for electrons and deuterium by changing the growth rates and phase of the ion driven turbulence, while lithium flux is always directed outward. A particle diffusion coefficient, D ~0.07 m^2/s, and an inward pinch velocity, V ~0.27 m/s, in qualitative agreement with Bohm-gyro-Bohm predictions have been inferred in pellet fuelled lithized discharges. Radio frequency heated plasmas benefit from cleaner plasmas with edge optimized conditions. Lower Hybrid waves penetration and current drive effects were clearly demonstrated at and above ITER densities thanks to a good control of edge parameters obtained by plasma operations with the external poloidal limiter, lithized walls and pellet fuelling. Flexibility and reliability of Electron Cyclotron Heating System allowed FTU contributing to ITER relevant issues such as MHD control: sawtooth crash was actively controlled and density limit disruptions were avoided by central and off-axis deposition of 0.3MW of EC power at 140 GHz. Fourier analysis shows that the density drop and the temperature rise, stimulated by modulated EC power in low collisionality plasmas are synchronous, implying that the heating method is the common cause of both the electron heating and the density drop. Perpendicularly injected ECRH, demonstrated to be more efficient than oblique's, reducing by a factor 3 the minimum electric field required at breakdown. Theoretical activity further developed the model to interpret high frequency fishbones on FTU and other experiments as well as to characterise BAE induced by magnetic islands in ohmic discharges. The theoretical framework of the general fishbone like dispersion relation was used for implementing an extended version of the HMGC hybrid MHD gyrokinetic code. The upgraded version of HMGC will be able to handle fully compressible nonlinear gyrokinetic equations and 3D MHD.

---

[*] See Appendix

1. Introduction

Since last IAEA-FEC in Genève [1], the progress in FTU operations with Liquid Lithium Limiter (LLL) has enabled increasing the range of plasma parameters accessible for high current plasmas with high density [2]. Besides its validity as a plasma facing component, the LLL demonstrated to be a powerful tool in controlling edge plasma conditions thus allowing plasma performances improvement and profiles optimisation. Moreover, the beneficial effect of the presence of lithium in the discharge, which triggers the density peaking was assessed by a microstability analysis [2]. A combination of clean plasma, low recycling-high edge temperature obtained by LLL and pellets injection allowed shaping FTU L-mode plasma density profiles to match those expected in ITER scenario 4: in these conditions Lower Hybrid waves penetrated the plasma core demonstrating for the first time a safe path to LH operations in ITER [3]. FTU has contributed in studying the breakdown assisted by ECRH [4] in the framework of a multi-machine effort [5]. Indeed, the pre-formation of a low density plasma enabling plasma current start-up with a reduced electric field is of the utmost relevance for ITER where a low in-vessel toroidal electric field, $E \leq 0.3$ V/m, will be available. The exploitation of ECRH capability in controlling MHD and disruptions continued in FTU and in collaboration with ASDEX-U team [6], the sawtooth frequency was controlled by modulated ECRH power and density limit disruptions were controlled both by central and at off axis power deposition (close to location of q=2 surface). ECRH operations in FTU also addressed the issue of particle confinement in presence of additional heating by probing plasma properties with modulated power. The theoretical framework of the general fishbone like dispersion relation (GFLDR) has been applied to construct a solid and systematic interpretative basis for electron-fishbone [7] and Alfvénic mode observations in FTU. The GFLDR framework has also been used for implementing an extended version of the hybrid MHD gyrokinetic code HMGC [8]. Applications of this eXtended HMGC (XHMGC) code [9, 10] range from FTU electron-fishbone to collective excitations of meso-scale Alfvénic fluctuations in FAST [11, 12], for which detailed transport analyses have been carried out [13].

2. High Density Discharges with Liquid Lithium Limiter

At last FEC in Genève, FTU reported on the improvement of plasma operations when using the Liquid Lithium Limiter. In particular better energy confinement time, up to $1.4 \cdot \tau_{ITER97-L}$, was found for the saturated ohmic confinement (SOC) regime with respect to pre lithium FTU discharges [1]. Lithized discharges always exhibit peaked density profiles, with density as high as 1.6 times Greenwald's value, but the transition to enhanced confinement appears only when density peaking factor overcomes a threshold value of ~1.8. Results shown in Genève were limited to 0.5 MA plasma current, as higher current discharges never reached the peaking threshold. New discharges recently obtained at $I_P = 0.7$-0.75 MA, $B_T = 7$ T, $q_{cyl} \sim 5$,

Fig. 2.1: *Energy confinement time vs line averaged density in ohmic FTU "lithized" discharges.*

reach densities up to 1.6 times Greenwald's ($\bar{n}_e \geq 3.5 \cdot 10^{20} m^{-3}$) with peaking factor larger than 2 [2]. These discharges confirm the spontaneous transition to an enhanced value of the confinement time in the SOC regime when the density peaking factor overcomes the
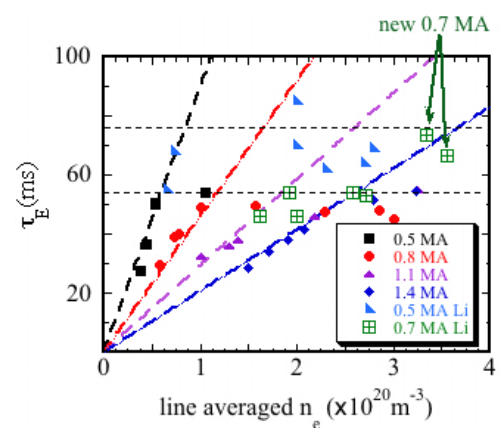
threshold value of ~1.8. In figure 2.1 a typical value of the confinement time of these discharges is added on the previous database.

Transport analysis with JETTO code, shows that in these discharges the electron thermal conductivity (χ_e)

TABLE I: #30582 PLASMA PARAMETERS @ r/a = 0.5

	t = 0.3 s				t = 0.8 s			
	$\overline{n}_e$ [10^{19}]	T [keV]	-a∇T/T	-a∇n/n	$\overline{n}_e$ [10^{19}]	T [keV]	-a∇T/T	-a∇n/n
D^+	3.21	0.47	2.14	0.89	15.50	0.26	4.606	3.118
e^-	6.03	0.57	3.07	0.89	15.95	0.24	4.943	3.118
Li^+	0.94	0.47	2.14	0.89	0.15	0.26	4.606	3.118

decreases as the density increases, while the ion thermal conductivity (χ_i) remains close to typical typical neoclassical value. A detailed microstability analysis of LLL discharges has been carried out with the GKW [14], and GS2 [15] codes to investigate the mechanisms leading to density peaking and improved confinement.
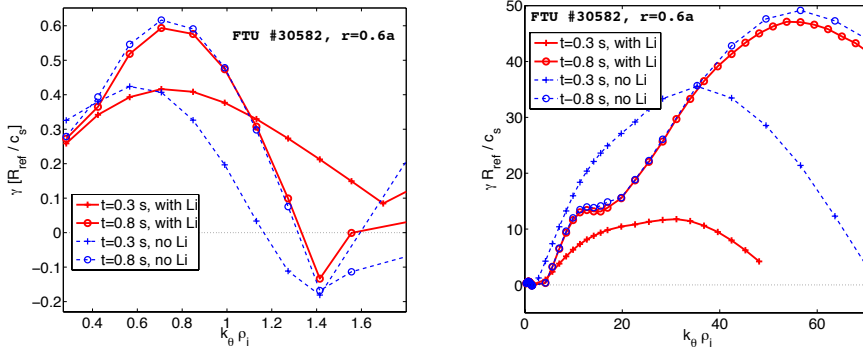

The parameters of FTU shot #30582 (typical LLL discharge) are reported in Table I for two selected time slices, at r/a = 0.6 (gradient region), during the high density phase when the deuterium and experimental

Fig. 2.2: *Growth rates of ITG (left) and both ITG plus ETG modes (right) for two time slices t = 0.3s and t = 0.8s at r = 0.6a for FTU shot #30582. Results with same parameters but without Lithium (dashed). Here $\rho_i = \rho_D$*

electron fluxes are found to change sign from inward (t=0.3 s) to outward (t=0.8 s). The other relevant parameters in the gradient region are: *t = 0.3s, q = 2.76, s = 1.62, α = 0.1, Z_{eff} = 1.9, Te/Ti = 1.2; t = 0.8s, q = 2.36, s = 1.5, α = 0.25, Z_{eff} = 1.06, Te/Ti = 0.92*. The growth rate of the linearly unstable modes at the two time slices, obtained by a full electromagnetic analysis is reported in the figure 2.2.

The particle fluxes driven by the unstable modes in the same region r/a = 0.6 and for same time slices are shown in figure 2.3. It is to be noted the different direction of ITG driven Li flux compared to that of e- and D at t = 0.3s, while at t = 0.8s all fluxes are in the same direction. The ETG driven flux is always inward for all
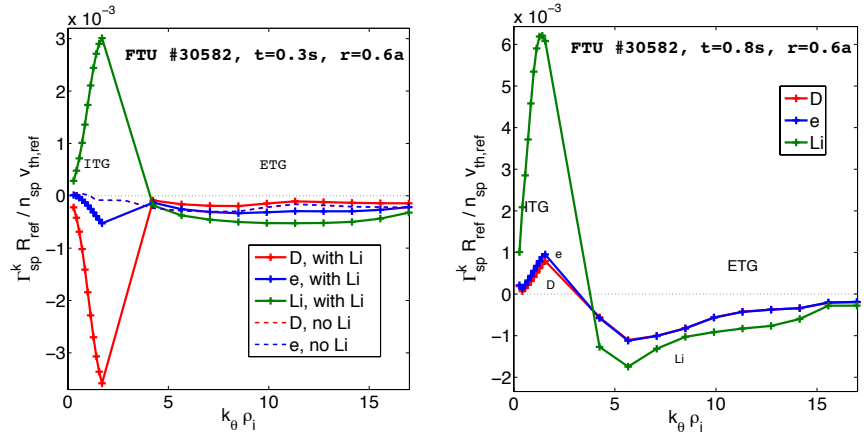

Fig. 2.3: *Spectrum of three species particle flux (red: D, blue: e⁻, green: Li) driven by ExB convection of ITG and ETG modes. Left t =0.3s, Right t = 0.8s. Results with the same parameters but without Li (dashed)*

species. As a consequence of the normalization scheme the fluxes shown in the figures above are just the initial values of the linear phase of the mode growth rate and carry no information about the saturated flux levels in the nonlinear phase. However, their sign does not change and determines the direction of the flux as the mode evolves.

The particle flux (linear) driven by the ETG modes is found to be inward (negative) for all the species and at both times. The particle flux driven by the ITG modes is inward for ions and electrons at t=0.3 s while it is outward (positive) for Lithium. The electron flux driven by ITG modes changes sign at t = 0.8 s becoming outward. By comparing the sign of the linear flux with the particle flux derived from the experimental data (JETTO analysis) it appears that the flux is dominated by short wavelength ion temperature gradient modes at mid radius in the gradient region of the discharge. Inside one third of the minor radius, at r/a=0.3, the ITG modes are found to be stable. The flux at t=0.8 s and r/a=0.3 is driven entirely by ETG modes and it is directed inward for all the particle species.

The linear microstability analysis above points out the importance of lithium to trigger a turbulent inward flux at mid radius of the discharge for electrons and deuterium by changing the growth rates and phase of the ion driven turbulence. The inward flux is sustained in the central region of the discharge through electron gradient dominated transport. The lithium flux in turn is found to be directed outward at plasma mid radius that is consistent with the low Z_{eff} value (close to 1.0) as measured during the high-density phase.

Fig. 2.4: *#32552, density profiles in the vicinity of two consecutive pellets*

High density discharges were also obtained by the first successful injections of D_2 pellets in presence of a significant wall lithization. Density profiles, for transport analysis, were obtained from the inversion of the FTU CO_2 scanning interferometer [16], which is a very powerful tool for studying fast evolution of density profiles and very strong gradients. Density profiles were taken every 62.5 μs with a spatial resolution of 1 cm and a line integrated density resolution $\Delta \bar{n}_e / \bar{n}_e \sim 2\%$. After a first density peaking, typical of pellet fuelled discharges, a further peaking is observed which suggests the existence of an inward pinch as seen also in gas fuelled discharges (figure 2.4).
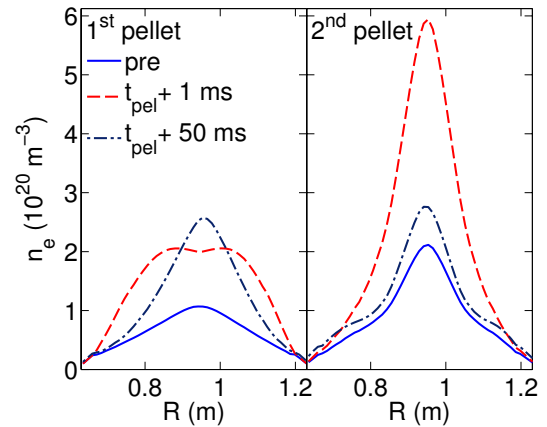

A fully interpretative transport analysis of the post pellet density profile decay has been performed in the region where there are no particle sources after the completion of pellet ablation (r/a < 0.5). According to particle conservation within each flux surface (S) and under the assumption that the particle flux can be expressed in terms of a

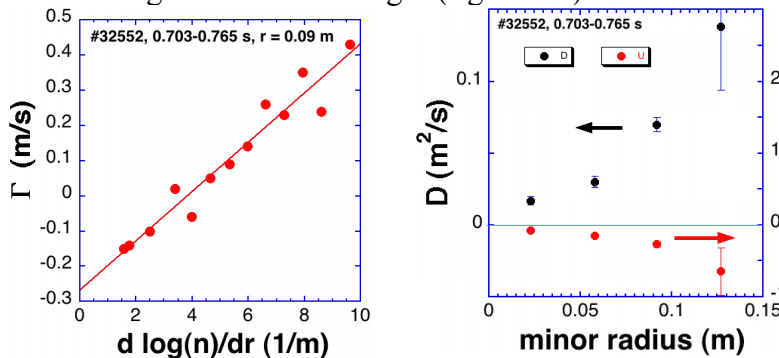*Fig. 2.5*: *Experimental particle flux at r = 9cm in the post pellet phase derived from density profiles evolution (left). Diffusion coefficient and pinch velocity versus minor radius (right)*

diffusive (D) and a pinch term (V), D and V can be determined at each radial position from a fit of the experimental data following the pellet transient. Indeed, at each flux surface, one can plot experimentally determined fluxes Γ (eq. b) versus the density normalized gradients at different times and get, from a linear fit, D and V.

$$a)\ \frac{\delta N}{\delta t} = S\,\Gamma \qquad b)\ \Gamma = \frac{1}{nS}\frac{\delta N}{\delta t} \qquad c)\ \Gamma = D\frac{\nabla n}{n} + V$$

Repeating the procedure at different radial positions, D and V profiles are found. (figure 2.5).

This technique gives, at r/a = 0.3, a particle diffusion coefficient of D ~0.07 m^2/s and an inward pinch velocity of V ~0.27 m/s in qualitative agreement with Bohm-gyro-Bohm predictions. An analysis of the density decay time in comparison with similar discharges of the pre-Lithium phase is in progress and further experiments are planned to produce new non-Lithized reference discharges. Finally, pellets have also been used in combination with Lower Hybrid waves (LH) for exploring new possibilities of driving plasma current at high density as described in the following section.

3. Lower Hybrid Current Drive at ITER relevant density

The lower hybrid current drive (LHCD) will potentially provide the most efficient tool for actively producing non-inductive current in tokamak plasmas, thus opening a path toward the realisation of a steady state reactor. The occurrence of the LHCD effect, in tokamak plasmas, has been confirmed indeed in many experiments, which, however, operated with densities, in the outer part of plasma column, markedly lower than those required for ITER.

New FTU experimental results have now assessed the plasma conditions enabling the penetration of the coupled LH waves power in the plasma and the consequent LHCD at plasma density even higher than that required on ITER [3, 17]. Although quasi-linear theory predicts that a properly coupled LH wave would fully propagate in the core of high density plasmas, recent experiments have shown no penetration or much stronger reduction of driven current than expected with increasing density. This effect already occurs for outer (*r/a*≈0.8) density even lower than that expected ITER [18, 19, 20]. In these experiments, the coupled LH power results indeed to be fully deposited at the very plasma edge when a certain threshold in the plasma density is exceeded. Similar effects are produced by

Fig. 3.1: *LH accelerated fast electrons hard X-ray vs plasma density. Unmodified edge (dashed lines) and high T$_e$ edge with lithized wall (full line) regimes.*

parametric instability (PI) observed in the early LH experiments aimed at the plasma core ion heating although other alternative or even concomitant mechanism can be envisaged. New experiments have been performed to modify FTU edge conditions, in very high density plasmas, to minimise the PI-produced spectral broadening [3]. The hard X-ray radiation produced by LH-accelerated supra-thermal electrons has been used to monitor the LH penetration and consequent effectiveness in driving current. Figure 3.1 shows how the hard X-ray emission, recorded along a central line of sight, varies with density. The experimental points connected by dashed lines refer to plasmas with three different sets of plasma current and magnetic field with non-optimised edge: the X-ray emission remains at the noise level for plasma density $\bar{n}_e \geq 1.0 \cdot 10^{20} m^{-3}$ (corresponding to: $n_{e0} \approx 1.5 \cdot 10^{20} m^{-3}$, and $n_{e\_0.8} \approx 0.4 \cdot 10^{20} m^{-3}$ at $r/a \approx 0.8$). In these conditions the coupled LH power appears to be fully deposited at the very edge of the plasma. It must be noted that in these discharges the launched LH spectrum, n$_{//peak}$ = 1.9, is accessible to plasma centre.

The edge conditions were then modified to produce higher temperature in the outer part of the plasma column, exploiting lithized wall, proper gas and pellet fuelling [3]. The experimental
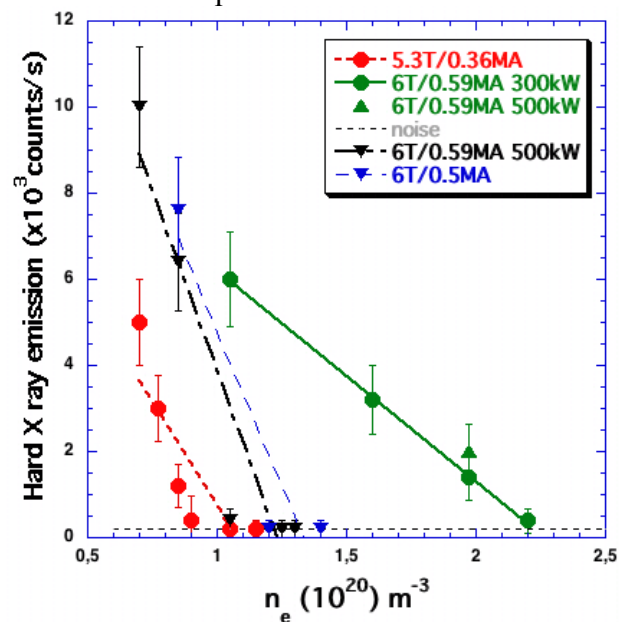
points connected by full lines in figure 3.1 refer to these conditions. As evident the LH penetration and CD is fully recovered at higher density: $\bar{n}_e \geq 2.0 \cdot 10^{20} m^{-3}$ (corresponding to: $n_{e0} \approx 5 \cdot 10^{20} m^{-3}$, and $n_{e\_0.8} \approx 0.85 \cdot 10^{20} m^{-3}$ at $r/a \approx 0.8$). Consistently with PI theory, a reduced spectral broadening is recorded in these conditions where $T_{e\_0.95} \geq 80 eV$, despite of the very high density plasmas. The very off axis electron temperature is estimated interpolating Thomson scattering measurements and Langmuir probes in the SOL. A width of about 7 MHz has been measured indeed at 35 db below the pump power peak, against the 15 MHz measured in lower density plasmas with unmodified edge conditions, where $T_{e\_0.95} \leq 50 eV$.

For sake of completeness data have also been compared with a linear model accounting for LH waves diffusion by density fluctuations in the scrape off layer [21]. Experimental spectral broadening, 10 db down the peak, is extremely well reproduced by this model, as shown in figure 3.2, although the aisles of the experimental spectrum appear broader, suggesting additional acting mechanisms. Only a detailed measurement of plasma periphery parameters and their gradients will allow discriminating between the relative weights of the different phenomena in preventing LH wave penetration. However, FTU experiments have shown that, by controlling edge conditions, LHCD
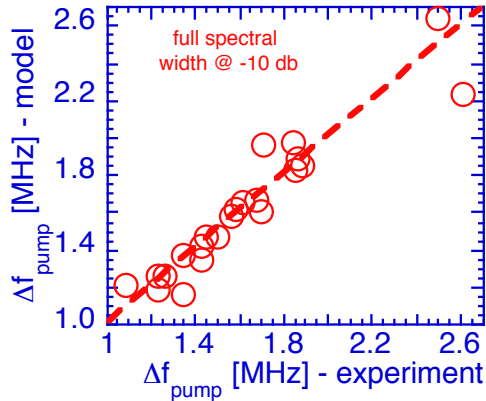
Fig. 3.2: Computed vs experimental LH pump frequency width at -10 db down the peak.

experiments can safely be designed for ITER in the full range of plasma densities relevant for a thermonuclear reactor plant.

4. ECRH studies

Experiments based of the exploitation of ECRH power have been carried out on FTU addressing ITER relevant issues, like: control techniques (sawtooth and disruptions), plasma formation (breakdown and start up) and plasma probing for transport studies.

Sawtooth (ST) Control is a critical issue for the plasma confinement [22], as large crashes can destabilize NTMs degrading plasma performance, on the other hand ST activity is useful in burning plasma to prevent ash accumulation in the plasma core.
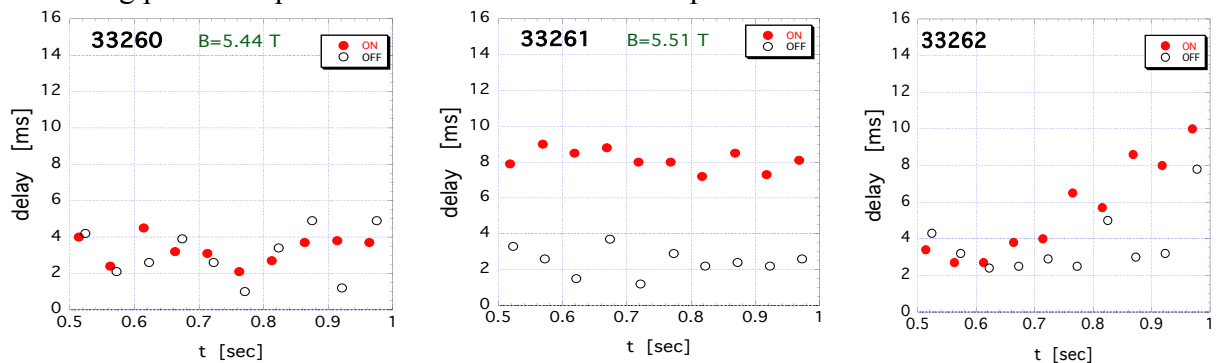

Fig. 4.1: Delay between sawtooth crash and ECRH switch on (red filled) and switch off (black empty). $P_{ECRH} = 0.77MW$, modulated: 10 ms on and 40 ms off

ST destabilization, already performed on FTU by non modulated ECCD [23], has been further investigated recently, using 500 ms of repetitive short pulses from 2 gyrotrons (0.770 MW), inducing the crash either by ECH and co-ECCD. A ramped toroidal field $B_T = 5.3 \rightarrow 5.9$ T allowed pushing the EC absorption radius r_{abs} inside the ST inversion radius r_{inv} (q = 1) up to $r_{abs} \sim r_{inv}/2$, to find the B_T value corresponding to ST crash induced by the EC trigger. Left

plot in figure 4.1 shows the effect of the ECH inside the inversion radius on the ST crash for $B_T = 5.44T$. The τ_{saw} is reduced by ~ 4 ms with respect to ST period with ECH just on the inversion radius (central plot). The plot on the right shows the combined effects on time delay of ECH+coECCD during the field ramping: the τ_{saw} is shortened for deposition inside r_{inv} up to t = 0.72 s still at ~4ms. Next experimental campaign will aim at controlling τ_{saw} at a specific chosen value.

Disruption avoidance by ECRH has been demonstrated in previous FTU experiments with off-axis ECRH in disruptions induced by Mo-injection [1, 24] and with on-axis ECRH in density limit disruptions [25]. In recent density limit experiments, disruption avoidance has also been achieved by injecting off-axis ECRH power (P_{ECRH}). The loop voltage has been used as a disruption precursor signal for ECRH real-time triggering. P_{ECRH} (140 GHz, $B_T = 5.3$ T) has been deposited at an off-axis

FIG. 4.2: *Time traces from top of I_P, $\bar{n}_e$ and P_{ECRH} in the reference density limit disruption (#32067) and in two discharges with off-axis ECRH (#32081, P_{ECRH} ~0.8 MW; #32086, P_{ECRH} ~0.4 MW)*

location (r_{dep} ~ 14 cm) compatible with the $q = 2$ surface ($r_{q=2} = 13 \pm 1$ cm): figure 4.2 shows the results for two discharges with different levels of P_{ECRH}. Note that, due to the lithium-conditioned walls, the Greenwald limit (~1.4×10^{19} m^{-3}) has been largely exceeded in these discharges. Taking into account that the fraction of absorbed power, computed by the quasi-optical ray tracing code ECWGB 3D [26], is roughly 25%, the absorbed *ECRH power sufficient for disruption avoidance is* $P_{ECRH} = 0.27 \pm 0.1$ MW. The disruption occurs as in the reference case (red curve) when the power is halved (black curve) or deposited too far from a rational surface (not shown).
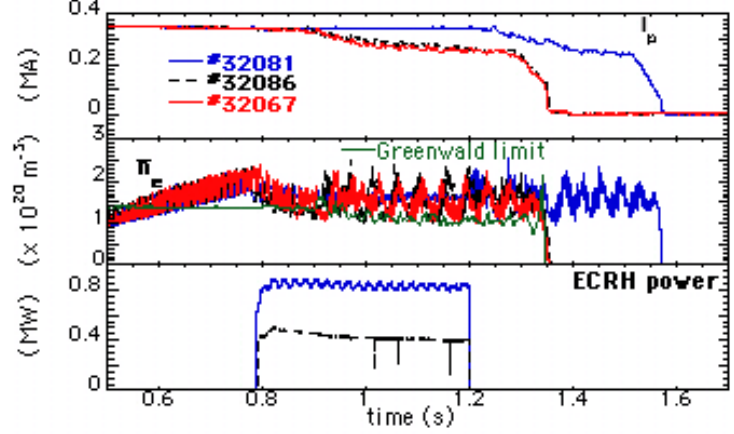
Probing of FTU L-mode ohmic discharges by modulated ECH shows that the central density drop and the resulting flattening of the density profile is not a by-product of plasma heating. Indeed, Fourier analysis of density and temperature time traces clearly shows that the density drop and the temperature rise in low collisionality plasmas are synchronous.
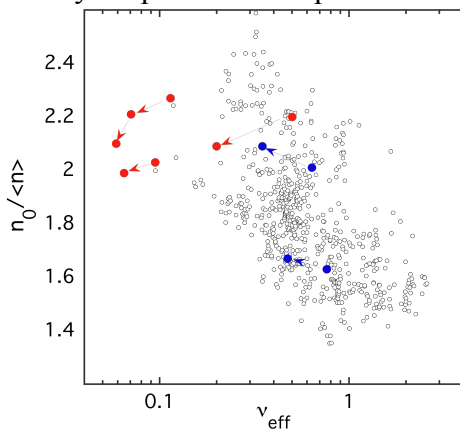

FIG. 4.3: *Density peaking vs ν_{eff} in OH FTU discharges ($B_T=6T$, $I_P=0.55MA$) (open gray symbols), EC heated discharges (red and blue dots). Arrows point from OH to RF heated phase*

This implies that the RF heating method is the common cause of both the electron heating and the density drop. The lack of delay between the time evolution of the density and the temperature excludes that T_e or the ratio T_e/T_i could be the cause of the flattening of n_e profile. The generation of an energetic tail in the electron distribution function sustained by the RF injection likely determines a spatial diffusion of the energetic electrons [27].

This would suggest that collisions, rather than density or T_e/T_i, are the key parameter of the density profile response to the ECH heating. Indeed we observe (figure 4.3) that, in FTU discharges with effective collisionality $\nu_{eff} \propto (z_{eff}<n> R/<T_e>^2) <1$, the density profile peaking, $n_0/<n>$, which in general increases by decreasing ν_{eff} [28, 29], decreases with the ECHR

power injection. When ν_{eff} is close to 1, on the contrary, the density peaking recovers its ohmic behaviour and the ECH power, by increasing T_e, reduces ν_{eff} and builds more peaked density profiles.

Experiments on ECRH assisted breakdown have been carried out on FTU, contributing to the multi-machine effort aiming at defining the optimum start-up scenarios for ITER [4, 5]. Using up to 800kW of EC power, the FTU plasma startup pressure has been increased by a factor 4 with respect to Ohmic values, while a minimum electric field of 0.4V/m at the breakdown, has been obtained for perpendicular EC injection (0°). A reduced efficiency is found for oblique injection (20°), which exhibits a lower plasma current ramp up rate and higher power to overcome radiation barrier: a factor 2 higher power is needed to obtain same results. This is likely connected with a positive effect of wall reflection in case of 0° injection that locally enhance the power. On the other hand 20° angle has better performance in generating pre-ionized plasma, with higher and wider electron density profiles. This is likely related to a different absorption mechanism of the XM polarization generated, for oblique propagating wave, after the first reflection from the wall. The EC assisted breakdown has been devoted also to reduce ohmic flux consumption. With off-axis EC resonances a faster current ramp is obtained with a reduction of 16% with respect to the central resonance position when a modest flux saving (6%) is due to the resistivity variation, consequence of higher T_e with ECRH. Changing toroidal field the resonance has been moved, inner or outer, at ~ 0.5 r/a; faster current ramp is obtained in both cases, with a further reduction of 16% in flux consumption with respect to the central resonance case. A strong reduction (factor 3) of plasma internal inductance during the current ramp up phase has been calculated from experimental pressure and equilibrium code reconstruction. This is in agreement with the observed faster current rise, even if more experiments are required to confirm the relationship between ECRH preionization and internal inductance reduction.

5. Theory and Modelling of Experimental Observations

The theoretical framework of the general fishbone like dispersion relation (GFLDR) has been applied to interpret evidence of high frequency fishbone at JET [30, 31] and to construct a solid and systematic interpretative basis for electron-fishbone [7] and Alfvénic mode observations in FTU.

A model based on overdriving a dynamic system near self-organized criticality has been proposed for qualitatively explaining (electron) fishbone bursting behaviour [32], which is observed with sufficiently strong perpendicular and parallel supra-thermal electron populations, generated by LHCD power and modelled by a quasi-linear ray-tracing code [33, 34]. Experimental evidences, meanwile, are provided by various tools: magnetic coils, soft-X ray, hard-

Fig. 5.1: *Spectrogram of the electron temperature fluctuations (top) and radial position (bottom) of the induced T_e fluctuations due to e-fishbones in FTU #20865*

X ray, ECE and by interpretative simulations with the JETTO transport code, constrained by magnetic reconstruction measurements. FTU experimental observations have provided the
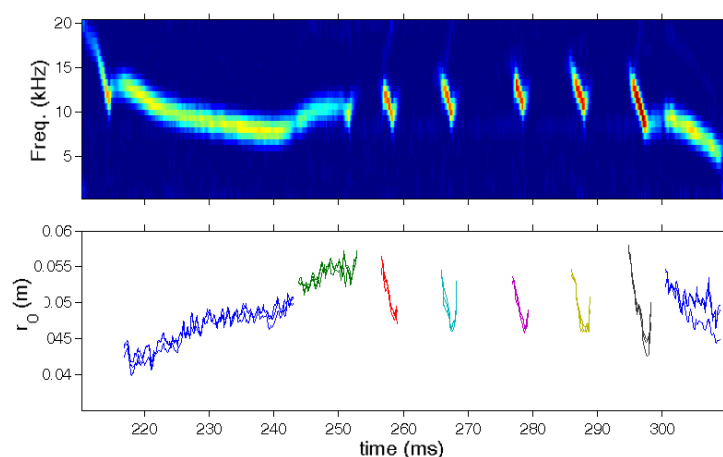
first evidence of strongly nonlinear behaviours in connection with electron fishbone excitations by LH only [30] and show clear evidence of fast electron redistributions [7]. These results suggest that the level of LH power input controls the transition from nearly steady state non linear oscillations (fixed point) to bursting electron fishbone oscillations (limit cycle) and that, in the bursting regime, the fishbone is an energetic particle mode (EPM) [35] well above marginal stability and associated with significant fast electron redistributions, analogous to the fast ion losses that are expected when ion fishbones are excited. Recently a new ECE analysis technique [36] has been applied to study the mode localization for the electron fishbone modes in both almost-stationary and bursting regime. Figure 5.1 shows that the e-fishbone induced T_e fluctuations drift outward in the almost-stationary regime, while they drift inward in the bursting regime. The "fixed point" mode seems to be saturating when the supra-thermal particle scattering out of the resonant region is continuously balanced by the source. Bursting appears with stronger drive, which pushes the system away from marginal stability and causes strong particle redistributions, slowly restored by sources. In other words, the strong regime is far from all descriptions based on proximity to marginal stability, which clearly do not apply at sufficiently strong drive, as shown in the original works on fishbones [37, 38] and confirmed more recently [39, 40]. More recently, FTU experiments studied fishbone-like modes with slightly reversed q-profile approaching the condition $q_{min} \approx 1$ and a marginally over-critical population of fast electrons produced by LH, aimed at exploring the critical threshold for mode destabilization [7]. New experiments are in progress in FTU to fully assess the electron fishbone phenomenology by higher LH power and different LH power waveforms, necessary for destabilizing modes at $q_{min} \geq 2$. Experiments are designed for producing higher supra-thermal electron tail temperatures via ECRH-LH synergy, yielding high pressure gradients for effective excitation of electron-fishbone in the high frequency range. The need of coupling LH power in the early phase of plasma current ramp, to match the desired q_{min}, make the experiment quite difficult. So far, it was possible to couple the available LH power in the range of 0.3-0.6MW during the plasma current ramp-up, by adopting a change in the FTU switching circuit and utilizing the new favourable operation conditions provided by the lithizated vessel facility. Next experiments will be aimed at increasing the LH power (above 0.8MW), in order to have an effective LH-ECRH synergy.
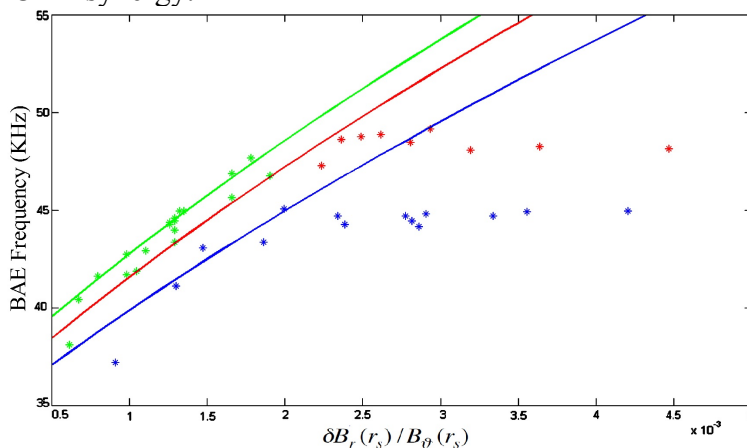

Fig. 5.2: *Observed and calculated BAE frequency as a function of island width ($\delta B_r(r_s)/B_\vartheta(r_s)$) for FTU shots 23184 (green), 25877 (blue) and 26644 (red)*

Beta induced Alfvén Eigenmodes (BAE) have been observed in DIII-D with strong neutral beam heating [41] during tearing mode in FTU and TEXTOR ohmic plasma [42, 43] and more recently with ICRH during a sawtooth cycle in ASDEX-U [44] and TORE-SUPRA [45], as well as in both Ohmic and ECRH plasmas in HL-2A [46], in connection with supra thermal electrons. BAE phenomena are generally very important to the understanding of dynamic behaviors of collisionless plasmas of fusion interest, for they occur in the low frequency kinetic thermal ion (KTI) [47] gap in the shear Alfvén wave (SAW) continuous spectrum, where various processes characterize the complex behaviours of burning plasmas on long time scales [48]. The GFLDR framework, usually

employed for discussing circulating thermal plasma particle kinetic compression effects on low-frequency SAW [49], has been adopted to discuss trapped thermal particle effects on the structures of the low-frequency shear Alfvén continuous spectrum [50], emphasizing their crucial roles for interpreting experimental observations [51, 52]. Recently, we also carefully reconsidered some long (> 200 ms) BAE observed in FTU [53]. As observed previously [42, 54] these are oscillations at frequencies between 30 and 50 KHz, accompanying tearing modes with frequency below 10 KHz and with intensities two order of magnitude less than tearing modes. BAE frequency scales mainly with the Alfvén velocity, and does not scale exactly with the Alfvén frequency [42]. They are characterized by two main frequency lines, which merge in a single line when the island oscillation frequency becomes very low. Mode analysis pointed out poloidal and toroidal mode numbers $|m| = 2$, $|n| = 1$. The BAE frequency lines have $|n| = 1$, the higher ones propagating in the same direction with respect to the island, while the lower lines propagate in opposite direction. The difference between the two BAE frequency lines is exactly twice the fundamental frequency of the tearing mode. The frequency difference can be explained as Doppler shift due to island rotation, so that BAE forms a standing wave composed by two waves propagating at opposite velocities in the island rest frame. Similar phenomenology has been observed also in TEXTOR [43] and in EL-H2 [46]. The spectrum obtained by the bicoherence analysis of magnetic coils signals, shows that the BAE and tearing oscillations always start with the same phase, thus, it confirms the strong coupling between the two modes when magnetic island is not locked. The observed BAE frequency in FTU is in agreement with theoretical predictions [54, 55], with the observed frequency just below the predicted BAE SAW continuum accumulation point and strong correlation between BAE and tearing mode. We observe that, during the first part of island growth, BAE frequency increases roughly linearly, in good agreement with theoretical prediction (solid line in figure 5.2); on the other hand a discrepancy is found for $\delta B_r(r_s)/B_\vartheta(r_s) > 10^{-3}$, where BAE frequency remains rather constant. Therefore, we can confirm that perturbative theory predictions [55] give consistent results only for low magnetic island amplitudes.

The GFLDR framework has also been used for implementing an extended version of the hybrid MHD gyrokinetic code HMGC [8], which simultaneously handles two generic initial particle distribution functions in the space of particle constants of motion. Applications of this eXtended HMGC (XHMGC) code [9, 10] range from FTU electron-fishbone to collective excitations of meso-scale Alfvénic fluctuations in FAST [11], for which detailed transport analyses have been carried out [13]. These investigations assume FAST equilibrium profiles as initial conditions, after the self-consistent dynamic formation of the FAST scenarios is obtained iteratively by interfacing several numerical tools: transport codes (JETTO and the CRONOS suite of codes, including NEMO and SPOT) and the ion

Fig. 5.3: *Energetic particle orbits in a ITER-like equilibrium configuration, produced by the new hybrid MHD-gyrokinetic code HYMAGIC*

cyclotron resonance heating (ICRH) full wave code TORIC, coupled with the quasi-linear solver SSFPQL, which accounts for both ICRH and negative neutral beam injection (NNBI) [13]. Before its use as numerical investigation tool for supra-thermal particle physics,
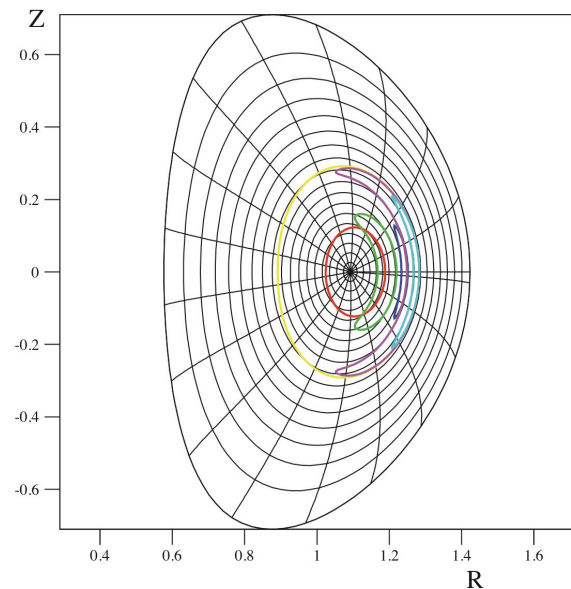
the XHMGC code has been verified against analytic theories [56] as well as global gyrokinetic codes, such as GTC, in common validity parameter regimes [57].

Strong efforts have focused on completing the implementation of the upgraded version of HMGC [8] to handle fully compressible nonlinear gyrokinetic equations and 3D MHD [58]. The new code HYMAGYC (HYbrid MAgnetohydrodynamics GYrokinetic Code) is built by interfacing a modified version of the CHEASE code [59] (equilibrium), an initial-value version of the original eigenvalue MHD stability code MARS [60] (field solver) and an originally developed gyrokinetic particle-in-cell module, yielding the energetic ion pressure tensor needed to close the MHD equations. Figure 5.3 shows typical energetic particle orbits in an ITER-like equilibrium configuration, produced by the new code HYMAGYC.

References

[1] TUCCILLO, A. A., et al, "Overview of the FTU results", Nucl. Fusion **49** (2009) 104013

[2] MAZZITELLI, G., et al., Paper EXC/6-3 this Conference

[3] CESARIO, R., et al. , Paper EXW/P7-02 this Conference

[4] GRANUCCI, G., et al., Paper EXW/P2-03 this Conference

[5] STOEBER, J., et al., Paper ITR/P1-25 this Conference

[6] ESPOSITO, B., et al., Paper EXW/10-2Ra this Conference

[7] CESARIO, R., et al., Nucl. Fusion **49** (2009) 075034

[8] BRIGUGLIO, S., et al., Phys. Plasmas **2** (1995) 3711

[9] WANG, X., et al., 2010 "An extended hybrid magnetohydrodynamics gyrokinetic model for numerical simulation of SAW in burning plasmas" submitted to Phys. Plasmas

[10] WANG, X., et al., Paper THW/2-4Ra, this Conference

[11] PIZZUTO, A. et al., Nucl. Fusion 50 (2010) 95005; and CRISANTI, F., et al., Paper FTP/2-4 this Conference

[12] CARDINALI, A., et al., Paper THW/P7-04, this Conference

[13] CALABRÒ, G., et al., Paper **THC/P2-05**, this Conference

[14] ROMANELLI, M., et al, Physics of Plasmas **14** (2007) 082305

[15] M. KOTSCHENREUTHER, M., et al, Comput. Phys. Commun. **88** (1995) 128

[16] CANTON, A., et al, Applied Optics **45** (2006) 910

[**17**] CESARIO, R., et al., Nature Communications, August 2010, **http://dx.doi.org/10.1038/ncomms1052**

[18] KIROV, K.K., et al., "LH Wave Absorption and Current Drive Studies by Application of Modulated LHCD at JET" Proceedings of the 36th European Phys. Society Conf. on Plasma Physics, Sofia, Bulgaria, 2009

[19] WALLACE, G., et al, "Observation of Lower Hybrid Wave Absorption in the Scrape-Off Layer of Diverted Tokamaks" Proceedings of the 18th Topical Radio Frequency Conference, 24-26 June 2009, Gent, Belgium

[20] CESARIO, R., et al., "Plasma edge density and LHCD in JET", Submitted to PRL

[21] PERICOLI-RIDOLFINI, V., et al., "LHCD Efficiency in Tokamaks and Wave Scattering by Density Fluctuations at the Plasma Edge", 37th EPS Conf. on Plasma Physics, Dublin (Eire) 21st-25th June, paper P5.176, and submittted to PPCF

[22] SAUTER, O., et al., Phys. Rev. Lett. **88** 2002 105001

[23] NOWAK, S., et al., 2005 Proc. 32th Conf. Controlled Fusion and Plasma Physics, ECA, Vol. **29C** P-4.034

[24] ESPOSITO, B. *et al., Phys. Rev. Lett.* **100** *(*2009) 045006 and PERICOLI-RIDOLFINI, V., et al., Nucl. Fusion, **47** (2007) 608

[25] ESPOSITO, B., et al., Nucl. Fusion **49** (2009) 065014

[26] NOWAK, S. and OREFICE, A., Phys. Plasmas **1** (1994) 1242

[27] ANDERSON, D., and LISAK, M., Phys. Fluids 27 (1984) 2477-2482

[28] ANGIONI, C., et Al, Nucl. Fusion 47 (2007) 1326

[29] TUDISCO, O., et Al., "Peaked Density Profiles and MHD activity on FTU in lithium dominated discharges", Proc. Int. Symposium on Plasma-Surface Interactions 2010, Toki, Gifu, Japan

[30] ZONCA, F., et al., Nucl. Fusion **47** (2007) 1588

[31] ZONCA F., et al., Nucl. Fusion **49** (2009) 085009

[32] MILOVANOV, A., V 2010 Europhys. Lett. **89** 60004

[33] CARDINALI, A., and ZONCA, F., Phys. Plasmas **10** (2003) 4199

[34] CARDINALI, A., et al., Phys. Plasmas **14** (2007) 112506

[35] CHEN, L., Phys. Plasmas **1** (1994) 1519

[36] GUIMARÃES-FILHO, Z. O., et al., "Evolution of the electron fishbone-like mode localisation during frequency jumps on Tore Supra", (11th IAEA Technical Meeting on Energetic Particles in Magnetic Confinement Systems, Kyiv, 2009), P10

[37] WHITE, R. B., et al., *Phys. Fluids* **26** (1983) 2958

[38] CHEN, L., WHITE, R. B., and ROSENBLUTH, M. N., *Phys. Rev. Lett.* **52** (1984) 1122

[39] ZONCA, F., et al., *Nucl. Fusion* **45** (2005) 477

[40] ZONCA, F., et al., (2007) arXiv:0707.2852v1

[41] HEIDBRINK, W. W., *Phys. Rev. Letters* **71** (1993) 895

[42] BURATTI, P., et al., Nucl. Fusion **45** (2005) 1446

[43] ZIMMERMANN, O., et al., "Coupling of Alfvén-like Modes and large 2/1 Tearing Modes at TEXTOR", (Proc. 32nd EPS Conf. on Plasma Physics, Tarragona, Spain 2005), ECA **29C** (2005) P4.059

[44] GARCIA-MUNOZ, M., *et al., Phys. Rev. Lett.* **100** (2008) 055005

[45] NGUYEN C., et al., "Excitation of beta Alfvén eigenmodes in Tore-Supra", Pl. Phys. Contr. Fusion **51** (2009) 095002

[46] CHEN, W., et al., Paper EXW/4-4Rb this conference

[47] CHEN, L., and ZONCA, F., *Nucl. Fusion* **47** (2007) S727

[48] ZONCA, F*., Int. J. Mod. Phys. A* **23** (2008) 1165

[49] ZONCA F *et al., Plasma Phys. Contr. Fusion* **38** (1996) 2011

[50] CHAVDAROVSKI. I. and ZONCA F., Plasma Phys. Contr. Fusion **51** (2009) 115001

[51] LAUBER, Ph., et al., Plasma Phys. Contr. Fusion **51** (2009) 124009

[52] ZONCA F, et al., 2010 "Kinetic structures of shear Alfvén and acoustic wave spectra in burning plasmas" submitted to J. Phys.: Conf. Ser.

[53] BOTRUGNO, A., et al., "Comparison between BAE observations at FTU and theoretical models", (Proc. 37th EPS Conf. on Plasma Physics, Dublin, 2010), P4.110

[54] ANNIBALDI, S., V., et al, Plasma Phys. Contr. Fusion **49** (2007) 475

[55] BIANCALANI, A., et al., "Continuous spectrum of shear Alfvén waves inside magnetic islands", (Proc. 37th EPS Conf. on Plasma Physics, Dublin, 2010), P4.109

[56] WANG, X., et al., 2010 "Theory and simulation of discrete kinetic Beta induced Alfvén eigenmode in Tokamak plasmas" to be published in Plasma Phys. Contr. Fusion

[57] DENG, W., et al., 2010 "Gyrokinetic particle simulations of reversed shear Alfvén eigenmode excited by antenna and fast ions", to be published in Phys. Plasmas

[58] VLAD, G. et al., 2009 11th IAEA Technical Meeting on Energetic Particles in Magnetic Confinement Systems, Kyiv, Sep. 21 - 23, (2009); 2010 ITM General Meeting, Lisbon, Sep. 13-15, (2010)

[59] LUETJENS, H., et al., Phys. Commun. **69** (1992) 287

[60] BONDESON A, et al., 1992 "Computation of resistive instabilities in toroidal plasmas" *IAEA Technical Committee Meeting on Advances in Simulation and Modeling of Thermonuclear Plasmas* (Montreal 1992) pp. 306-315

Appendix: Members of FTU Team

B. Angelini 1), M. L. Apicella 1), G. Apruzzese 1), E. Barbato 1), F. Belli 1), A. Bertocchi 1), W. Bin 2), L. Boncagni 2), A. Botrugno 1), G. Bracco 1), S. Briguglio 1), A. Bruschi 2), P. Buratti 1), G. Calabrò 1), A. Cardinali 1), C. Castaldo 1), S. Ceccuzzi 1), C. Centioli 1), R. Cesario 1), C. Cianfarani 1), S. Cirant 2), R. Coletti 1), F. Crisanti 1), O. D'Arcangelo 2), M. De Angeli 2), R. De Angelis 1), L. Di Matteo 1), C. Di Troia 1), B. Esposito 1), G. Fogaccia 1), D. Frigione 1), V. Fusco 1), L. Gabellieri 1), A. Garavaglia 2), E. Giovannozzi 1), G. Granucci 2), G. Grossetti 2), G. Grosso 2), F. Iannone 1), H. Kroegler 3), M. Lontano 2), G. Maddaluno 1), M. Marinucci 1), D. Marocco 1), G. Mazzitelli 1), C. Mazzotta 1), A. Milovanov 1), F. C. Mirizzi 1), G. Monari 1), A. Moro 2), S. Nowak 2), F. P. Orsitto 1), D. Pacella 1), L. Panaccione 3), M. Panella 1), V. Pericoli-Ridolfini 1), S. Podda 1), A. Pizzuto 1), G. Pucella 1), G. Ramogida 1), G. Ravera 1), A. Romano 1), G. Ramponi 2), C. Sozzi 2), E. Sternini 1), A. A. Tuccillo 1), O. Tudisco 1), E. Vitale 1), G. Vlad 1), V. Zanza 1), M. Zerbini 1), F. Zonca 1), M. Aquilini 1), P. Cefali 1), E. Di Ferdinando 1), S. Di Giovenale 1), G. Giacomi 1), F. Gravanti 1), A. Grosso 1), V. Mellera 2), M. Mezzacappa 1), V. Muzzini 2), A. Pensa 1), P. Petrolini 1), V. Piergotti 1), B. Raspante 1), G. Rocchi 1), A. Sibio 1), B. Tilia 1), C. Torelli 1), R. Tulli 1), M. Vellucci 1), D. Zannetti 1)

1) Associazione Euratom-ENEA sulla Fusione, C. R. ENEA Frascati, Via E. Fermi 45, 00044 Frascati, Roma, Italy
2) Associazione Euratom-ENEA sulla Fusione, IFP-CNR, Via R. Cozzi 53, 20125 Milano, Italy
3) Associazione Euratom-ENEA sulla Fusione, CREATE, Via E. Fermi 45, 00044 Frascati, Roma, Italy